small NANO MICRO

Encoded Multichromophore Response for Simultaneous Label-Free Detection

*Constantin Pistol, Vincent Mao, Viresh Thusu, Alvin R. Lebeck, and Chris Dwyer**

The self-assembly of molecularly precise nanostructures is widely expected to form the basis of future high-speed integrated circuits, but the technologies suitable for such circuits are not well understood. In this work, DNA self-assembly is used to create molecular logic circuits that can selectively identify specific biomolecules in solution by encoding the optical response of near-field coupled arrangements of chromophores. The resulting circuits can detect label-free, femtomole quantities of multiple proteins, DNA oligomers, and small fragments of RNA in solution via ensemble optical measurements. This method, which is capable of creating multiple logic-gate–sensor pairs on a $2 \times 80 \times 80$-nm DNA grid, is a step toward more sophisticated nanoscale logic circuits capable of interfacing computers with biological processes.

Keywords:
- chromophores
- DNA
- logic gates
- resonance energy transfer
- sensors

1. Introduction

The self-assembly of nanoscale logic circuits has great potential as an economical and massively parallel method to create computer systems, and will play an increasingly important role in technology as the resolution and manufacturability of current microelectronics processes begin to reach fundamental limits. In this context, DNA self-assembly has the potential to expand the domain of conventional computer systems to reach into environments and application domains that are otherwise impractical, such as single-cell sensing or monitoring of microenvironments.

The potential for new application domains is a driving factor in the development of many molecular-scale computational devices.[1] Initial reports of molecular logic consist of switches and basic Boolean logic gates,[1–4] with more recent developments demonstrating molecules or molecular ensembles capable of implementing a variety of logic functions[5–7] in a range of chemical environments, including cellular contexts.[8–10] Scaling these devices to more complex systems is a challenge because they often use incompatible chemical inputs and outputs or multiple representations for binary signals. Optical switches,[11–13] logic elements,[14,15] and waveguides[16,17] are promising candidates for interfacing biology and computation, but the interconnectivity of individual devices remains a challenge.[1]

Herein, we demonstrate a method of sensing that uses DNA self-assembly to integrate and precisely organize collections of chromophores into resonance energy transfer (RET) gates with the ability to detect label-free biomolecules in small volumes at the nanoscale. Results are presented which demonstrate that such gates can be operated similarly to conventional logic and, in an example application, can detect femtomole quantities of analytes such as proteins and short nucleic acids. The method can be combined with other fluorescence resonance energy transfer (FRET)-based sensors[18–21] and is detectable by ensemble optical measurements with a dual-excitation-beam spectrofluorometer, thus enabling high-throughput assays, unlike previously demonstrated surface-bound atomic force microscopy (AFM)[22] and nanowire[23–27] detection methods. Furthermore, the method enables input and output encoding, which increases the number of sensors within a diffraction-limited spot orthogonal to what is possible with simple wavelength-multiplexed sensing.

[*] Prof. C. Dwyer, Dr. C. Pistol, V. Mao, V. Thusu
Department of Electrical and Computer Engineering
Duke University
130 Hudson Hall
Durham, NC 27708 (USA)
E-mail: dwyer@ece.duke.edu
Prof. A. R. Lebeck
Department of Computer Science
Duke University
Box 90921, Durham, NC 27708 (USA)

Supporting Information is available on the WWW under http://www.small-journal.com or from the author.

DOI: 10.1002/smll.200901996

2. Results and Discussion

2.1. Encoding the Optical Response of Multiple Sensors

Hierarchical DNA self-assembly is used to create nanoscale grids on which chromophores can be precisely patterned. Figure 1b and c shows AFM images of a $2 \times 80 \times 80$ nm DNA grid assembled using 4×4 tile motifs.[28] Briefly, we assemble each of 16 tiles independently and design the DNA sticky-ends such that each tile will bind at only one position in a 4×4 grid (Supporting Information, Section 2.2). Since each tile is formed independently, we can selectively functionalize the DNA strands and after grid assembly form a precise chemical pattern. We use 5'-SH end functionalization to conjugate commercially available chromophores at precise locations on the grid (Supporting Information, Section 2.1).

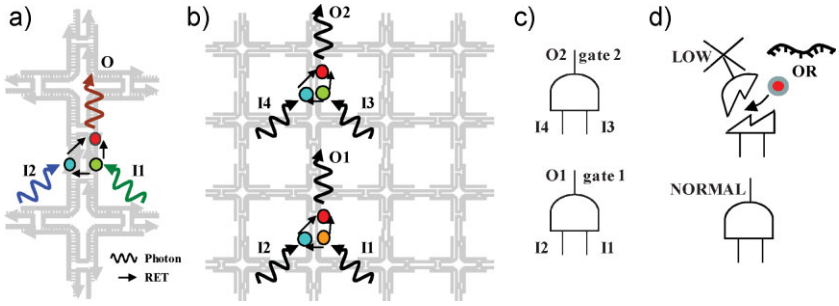

Figure 2. a) Chromophores are attached to the 5′ and 3′ ends of shell strands with input (I) chromophores on one tile and the output (O) on the neighboring tile. The inputs and the output are separated by the five-base-pair intertile sticky-end. b) Two gates are placed on the 16-tile grid structure to show proof-of-concept, but in principle this method can place 24 gates. c) Input and output encoding creates an abstract collection of distinct logic gates. d) Analytes bind to specific gates, which eliminate (or reduce) the output.

RET of grid-bound chromophores is used to create constrained pathways for excitons to transfer between donors and acceptors. The output is detected by observing a multi-donor RET index, which changes due to the input excitation or condition of the gate (e.g., by denaturation). In this work, we investigate chromophore "triplets" (i.e., two donors–one acceptor) for logic and sensing behavior. The optical response of a triplet can be tuned by changing donor–acceptor separations on the DNA grid such that a specified number of donor inputs (one or two) must be excited to generate a given level of acceptor fluorescence. Abstractly this is a Boolean AND gate, which requires the precise placement of chromophores at distances comparable to the Förster radius, R_0, of each pair. Since DNA nanostructures can organize chromophores at resolutions comparable to the helical pitch (3.4 Å), a DNA grid is well suited to this purpose.

Sensing is demonstrated with two RET gates on a DNA grid (Figure 2). Analyte receptors (e.g., complementary DNA, locked nucleic acid (LNA), or biotin) are placed at intersections between tiles to disrupt each gate output through competitive binding between the structural DNA sticky-ends and the analytes. The disruption of the gate is observable through a change in fluorescence output and will depend on the extent to which the analyte can disrupt the gate. Since the specific site to which an analyte binds will determine its ability to disrupt the gate, we expect different output for different analytes. As a proof-of-concept we detect 26-nucleotide (nt) DNA, 5-nt RNA, and streptavidin as representative biomolecules of interest (e.g., miRNAs, metabolic proteins).

In principle, arbitrary numbers of input and output chromophores can be chosen for triplets (gates) that respond in distinct spectral bands. However, in practice this number is restricted by the availability of real chromophores that are compatible in a biological setting and are also viable RET pairs. Furthermore, spatial "encoding" can achieve larger numbers of distinguishable triplets by lateral separation but is diffraction limited without the aid of super-resolution techniques, which also place important additional restrictions on triplet composition.

To increase the number of sensors that can be spectrally resolved beyond the above limits, inputs and outputs must be encoded such that they share the same optical band yet are independently discernible. To achieve this, triplets are designed such that: 1) input chromophores have globally unique excitation bands, and 2) output chromophores emit with distinct intensities. Although it is possible to also choose output chromophores that emit at distinct wavelengths, we avoid this approach since it is constrained by the above limitations.

2.1.1. Encoding Inputs

Inputs are designed to enable wavelength-multiplexed addressing of each gate. Only when both input chromophores are excited is an appreciable degree of RET observed from the output. For example, gate 1 in Figure 2b has inputs I1 and I2, which must both be excited for appreciable RET to the output chromophore (O). Since gate 2 in Figure 2b has a different set of input chromophores, it is weakly excited when gate 1 is selected and vice versa.

The criterion for minimally distinguishable gate response is defined by considering the output of two gates that have identical input chromophores except for one. This represents the limiting case, analogous to a Hamming distance of one in information

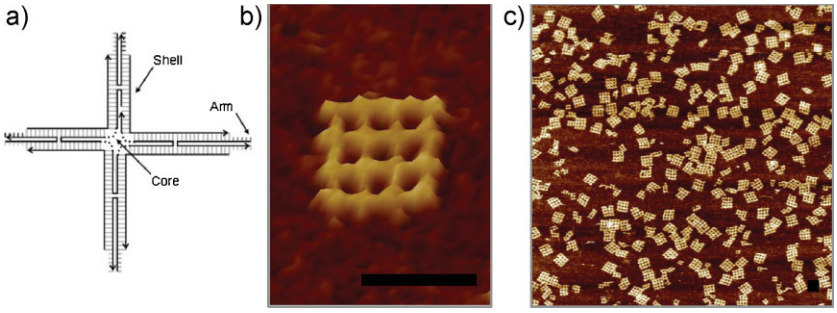

Figure 1. a) Tiles are assembled from nine DNA strands that present unique sticky-ends on each arm. b,c) AFM images of grid structures composed of 16 tiles. Scale bar: 60 nm.

NANO MICRO small

coding theory, and is the worst-case scenario for disambiguating the output from two distinct gates. Thus, to demonstrate that the method can operate at this limit, we show single gate selection between two gates that share one type of input chromophore and have a distinct remaining input. (The common input for both gates is Alexa Fluor 532. The unique inputs are Pacific Orange for gate 1 and Oregon Green for gate 2.)

2.1.2. Encoding Outputs

A method is introduced to design outputs, which enables encoding of multiple gates in the same output spectral band. This is achieved by designing each triplet output to emit at a distinct intensity such that the combined intensity of all gates uniquely identifies the logical result of each gate. For example, gate 1 and gate 2 in Figure 2b use the same output chromophore and the only distinguishing characteristic is the output intensity. The intensities must be tuned to enable identification of all four possible results for the two gates (00, 01, 10, 11).

The criterion for tuning output intensity is based on the mathematical foundation of unique prime factorization of integers. By choosing a logprime weight for each output intensity, the superposition of responses is unique, as given by:

$$\sum_{i=0}^{N-1} \log(W_i) \tag{1}$$

where W_i is prime. The proof of this is straightforward by analogy to the factorization of integers into primes and the exponential relationship between logarithms and sums. Thus, the sum of the logarithms of N distinct prime numbers is unique. For example, if gate 1 is tuned based on log (2) and log (3) (0 and 1, respectively) and gate 2 is tuned based on log (5) and log (7) (0 and 1, respectively), the linear combination of any two output values yields a unique value over the entire space of binary outputs and uniquely identifies the value of each gate output.

Tuning the intensity of each triplet output is accomplished by changing the tether that links the output chromophore to the 5' sticky-end on the DNA grid. We explore five different tethers: ''Std'' (i.e., S6), S3, S9, S18, and ''Neg'' (which uses a 1-nt shorter shell strand). Each tether is a commercially available thiol linker with spacers attached at either the 5' or 3' phosphate of a synthetic oligonucleotide. Chromophore functionalization to the end of the tether is performed the same as described previously. We make no assumptions about the distance at which a given tether ''holds'' a chromophore, since we have observed nontrivial association of chromophores with nearby nucleic acids that cannot be explained by a simple separation argument.

Encoding the optical response of multichromophore triplets provides a multiplicative increase in the number of unique sensors that can be resolved within a single diffraction-limited spot. The total number of unique sensors our system could employ per spot is $\binom{n}{k} \cdot q$, where n is the number of available input chromophores, k is the number of inputs to each gate, and q is the number of unique output tethers.

2.2. Simultaneous Detection of Label-Free Analytes

To implement logic we use wavelength-division multiplexing to selectively excite donors, which represent inputs to our system. A donor input is excited by the absorption of a photon and transfers this energy to a nearby acceptor. Upon excitation by RET, the acceptor relaxes by spontaneous emission of a photon with lower energy. The relative intensity of acceptor fluorescence between two narrow bands serves as the RET index (I_{RET}), as derived in the Supporting Information. I_{RET} can be calculated from the observed ensemble steady-state fluorescence at two wavelengths, and can yield detailed information about time-averaged donor–acceptor configurations (e.g., $\kappa^2_{x,y}$ and $r_{x,y}$) by standard nonlinear least-squares fitting. Later, we show how a change in I_{RET} (i.e., $\Delta I_{RET} = [I_{RET}(\text{final}) - I_{RET}(\text{initial})]/I_{RET}(\text{initial})$) is an output indicator for our logic gates and how such systems can be multiplexed to detect distinct molecular species in solution.

It was found that the DNA grid must be partially melted to make the target site near the gate output labile to analyte. In the presence of an analyte, and upon heating (37 °C) and annealing back to low temperature (18 °C), we observed the change in I_{RET} using two 10-nm-wide spectral windows centered on $\lambda_1 = 553$ nm and $\lambda_2 = 589$ nm for each gate's output chromophore to conclusively identify any analytes present in the solution (Figure 3). This RET index can be modified to use the signal from the emission bands of both input chromophores (i.e., donors) when there is no overlap between the donor excitation and emission bands. This only holds for the tether and dual-gate experiments described later, in which case an additional I_{RET} term is added to capture the band.

Since the DNA sticky-ends may displace the analyte upon annealing, we choose either a receptor with very high affinity (e.g., biotin for streptavidin), design the sticky-ends to be fully complementary to the analyte (e.g., DNA), or use LNA which can selectively enhance nucleic acid binding (e.g., for detecting small RNA).

An analyte can be detected by this method if its dissociation rate constant (K_D) is comparable to or smaller, due to the partial melting process, than the sticky-end dissociation rate constant at room temperature. We approximate the cooperative sticky-end dissociation rate constant by:

$$K_D = \exp\left[\frac{\Delta H_1 + \Delta H_2}{RT}\left(\frac{1}{T_{m1} + T_{m2}} - \frac{1}{T}\right)\right] \tag{2}$$

where ΔH_1, ΔH_2, T_{m1}, and T_{m2} are defined by the two 5-nt sticky-ends holding the gate output chromophore near the inputs and are estimated by the nearest-neighbor model[29] ($K_D \approx 10^{-1}$). The actual dissociation rate constant must be smaller than this, since we observe many intact grid structures at room temperature; however, longer-range cooperative interactions along the DNA helix are ignored in this approximation.[30] In the case of DNA sensing, the 26-nt analyte strands have two 5-nt regions at each end that are complementary to the sticky-ends of either gate. Since the sticky-ends have the same dissociation rate as the regions of

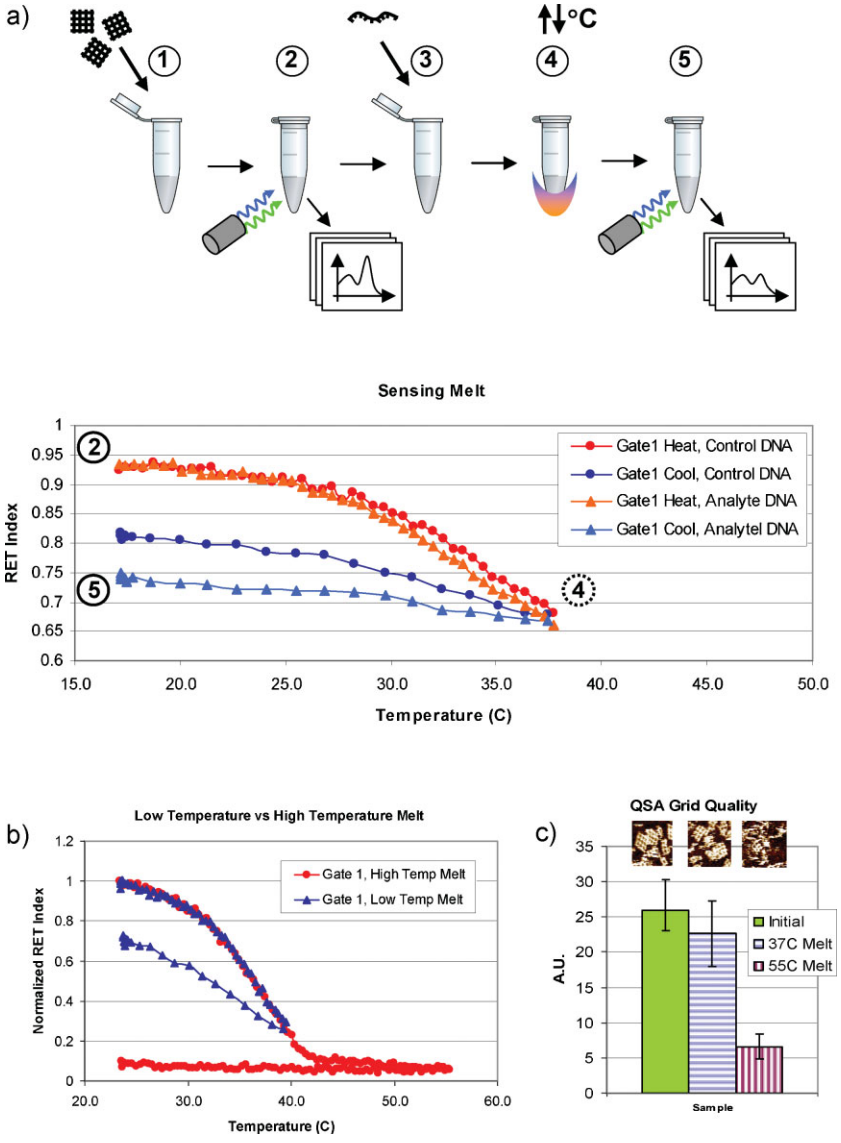

Figure 3. Overview of the sensing process. DNA grids (1) with attached chromophores are added and an initial optical readout of all gates is performed (2). After adding the analytes (3), the sample is heated (4) to 37 °C (12 min) and subsequently cooled back to 18 °C (30 min) using two baths and closed-loop temperature feedback to ensure repeatability. A final optical readout is performed (5), the I_{RET} values are calculated for each acquired spectrum, and the relative variation from initial values is recorded (ΔI_{RET}). The RET index variation of gate 1 in a grid with the two-gate configuration is shown in (a). Two samples are continuously monitored, one including the target analyte (e.g., single-strand DNA) for gate 1 and one including a control strand. The I_{RET} drops as the temperature increases, (2) to (4). After cooling, the control sample shows higher I_{RET} than the sample with target analyte present. Increasing the melting temperature to 55 °C shows an irreversible drop in I_{RET}, which suggests structural damage (b) (control data corrected for fluorescence level and temperature dependence: see the Supporting Information, Section 4.1). The same conclusion is supported by AFM analysis in (c), where the QSA metric shows a small decrease in grid structure quality after the low-temperature melt and a large degradation after the high-temperature melt.

the analyte that bind, non-Watson–Crick interaction between the middle of the analyte strand and the surrounding DNA is the likely cause of a reduced dissociation rate after the partial melt. Thus, the analyte strand is detectable and we also show that the binding of the 5-nt end regions to the sticky-ends is sequence specific. In the case of RNA sensing, the 5-nt analyte strand is complementary to only one (LNA) sticky-end near the gate output. Since RNA–LNA interactions are stronger than identical LNA–DNA interactions,[31,32] the 5-nt RNA analyte can successfully displace the complementary DNA sticky-end and thus be detected. In the case of protein sensing, the streptavidin–biotin dissociation rate ($K_D \approx 10^{-15}$)[33,34] is substantially smaller than the DNA sticky-end dissociation rate and easily detectable. To facilitate gate-output disruption, we use three biotins (attached to three shell strands; see the Supporting Information) in the 8-nm^3 vicinity of the chromophores. However, the supporting AFM data (see Figure 4) show that one or two proteins bind to any single gate, which is most likely due to steric occlusion by the ≈4-nm-wide streptavidin.

Control experiments indicate that non-competing (i.e., noncomplementary) nucleic acids (DNA or RNA) do not appreciably change I_{RET}. The change in I_{RET} noticeable in the control shown in Figure 3b is most likely due to nonspecific structural rearrangement of shell strands during the annealing step. Since this change is less than the change observed when an analyte is present, it can be baselined. Noncompeting proteins, such as bovine serum albumin (BSA), show a noticeable modulation but do not interfere with the binary discrimination of any analyte identity because it too changes I_{RET} by a small fraction. A likely explanation is that nonspecific interactions between the hydrophobic regions of the chromophores, DNA, and BSA change the helical conformation near the gate and thus modulate I_{RET}. Furthermore, we found that nonspecific fragmentary RNA (5-nt) does not appreciably modulate I_{RET} at non-LNA sticky-end sites.

Since partially melting the grid can also lead to disruption of the AND gates, even without analyte, we first characterize this disruption by monitoring I_{RET} during the melt and determining the post-melt structural yield of the grids by AFM. Yield information is derived from AFM images of DNA lattice structures by counting the number of square cavities in a given image relative to the coverage of DNA and normalizing the result to an idealized case of perfectly formed structures (Supporting Information, Section 3). We call this metric the quality of self-assembly (QSA). We found that melting to 37 °C does not appreciably disrupt the grid structure, and yields a 14% change in I_{RET} upon reannealing and a 12% change in QSA, while still making the analyte binding site accessible.

NANO MICRO small

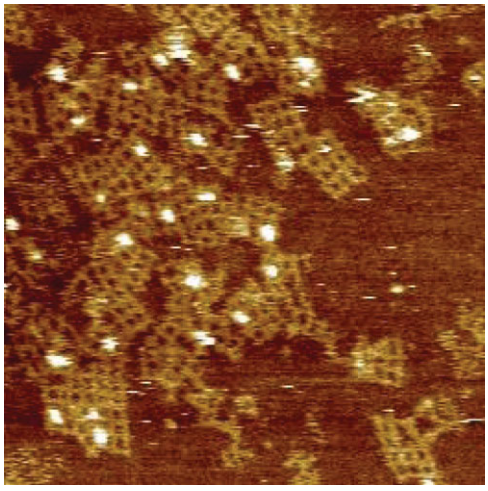

Figure 4. AFM image ($1 \times 1\ \mu m^2$) of dual-gate 4×4 DNA grids with bound streptavidin (16 nM grid, 32 nM streptavidin, 1×tris-acetate–EDTA (TAE)/Mg^{2+} buffer).

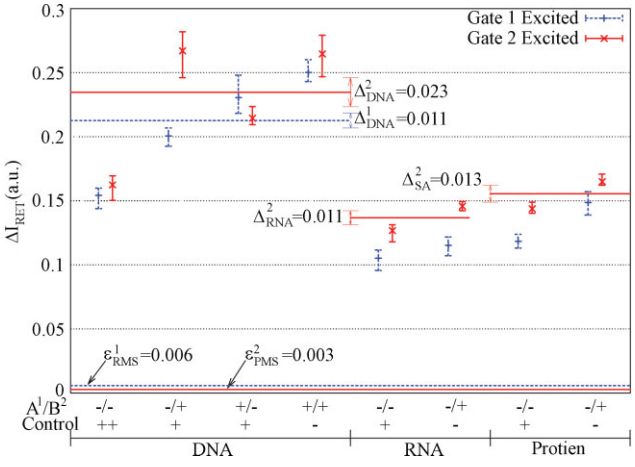

Figure 5. Two-AND-gate response across DNA, RNA, and protein analytes. Gate 1 is designed to be sensitive to analyte A (A_1) and gate 2 to analyte B (B_2). For DNA sensing, A, B, and the control are 26-nt DNA strands (Supporting Information, Section 2.3). For RNA sensing, B and the control are 5-nt RNA strands (Supporting Information, Section 2.4) where gate 2 is modified to include an LNA sticky-end. For protein sensing, B is streptavidin and the control is BSA, where gate 2 is modified to include a biotin unit next to each chromophore.

Figure 5 presents the response of the two-AND-gate system while varying the analyte conditions and input excitations that target each gate. The averages in Figure 5 are derived from the change in ΔI_{RET} across four identical experiments made from the same stock of triplets. Due to strand rearrangement, we observed a marked change in I_{RET} from the variability in the time–temperature profile used during the sensing process. Thus, the error bars in Figure 5 are derived from the same experiments and show the minimum and maximum change in ΔI_{RET} after uniformly removing one outlier (i.e., the sample farthest from the average) from each data set to eliminate the artifact of time–temperature profile variability. Since the outlier removal process is blindly applied to the four experimental runs (per analyte), it cannot introduce any bias. Future work will investigate methods to reduce the required number of replicate experiments (e.g., four in this case). Horizontal lines are drawn to indicate the ΔI_{RET} value that serves as the binary decision threshold to determine the presence of an analyte. The noise margin for both gates is about $2\times$ (Δ^1 and Δ^2). This change in signal is sufficiently larger than the background noise to make a 100% determination of each analyte.

The noise margin around each decision threshold (Δ^1 and Δ^2, respectively) is shown for comparison to the root-mean-square (RMS) noise for each gate (ε^1 and ε^2, respectively). For DNA sensing there are two thresholds corresponding to each gate's sensing decision. For the RNA and protein experiments, a single threshold is used since only one gate is selectively targeted (gate 2). The ΔI_{RET} threshold for all analytes is above the noise floor and is reproducible.

We also characterized the sensitivity of the system to various analyte concentrations, to determine the detection limit and feasibility of using ΔI_{RET} to deduce an activity factor and the concentration of each analyte. Figure 6a shows the observed change in I_{RET} for gate 1 and gate 2 as a function of concentration for the DNA analyte (26-nt) that targets gate 2. In practice, the ratio of analyte to a fixed concentration of DNA grid (4 nM) is varied to achieve different analyte concentrations. We determined the limit of detection for our setup by finding the analyte concentration at which we could no longer distinguish between the two gate outputs. We found that with a commercial charge-coupled device (CCD) spectrometer and short exposures (≈2 min), the detection limit is approximately 4 nM at an analyte-to-grid ratio of 1:1. We estimate our observation volume to be 25 μL by geometric arguments (Supporting Information, Section 4.2), and thus can detect a lower limit of 8 fM of DNA analyte. Single-photon detection methods will further reduce this detection limit by enabling few- and single-grid measurements. By using a minimum concentration of grid, as limited by the sensitivity of the optical setup, the concentration of analyte can be in excess and thus maximize the binding activity and observed change in I_{RET}.

Figure 6a shows that the change in I_{RET} is monotonic in concentration, which indicates, over the range of 4 to 240 nM, that the gate output is useful for estimating analyte concentration. However, these data must be compared against a calibrated sample and thus limit the usefulness of the approach for "blind" concentration measurements without further study. We also characterized the feasibility of using output tuning to create unique pairs of gates that share an output chromophore. The top panel in Figure 6b shows the output response (ΔI_{RET}) for each of the five tethers undergoing a sensing operation on a single gate designed to detect a DNA analyte.

We demonstrate how distinct tethers can be used to encode gate response by building a two-gate nanostructure as described above, but with the modification that one gate uses the S18 tether and both share the same kind of input and output chromophores (i.e., rhodamine red). In principle, the status of each gate should be masked by the other if the output tethers cannot uniquely encode the response of each gate to analytes. Figure 6c shows the average ΔI_{RET} for each gate under various

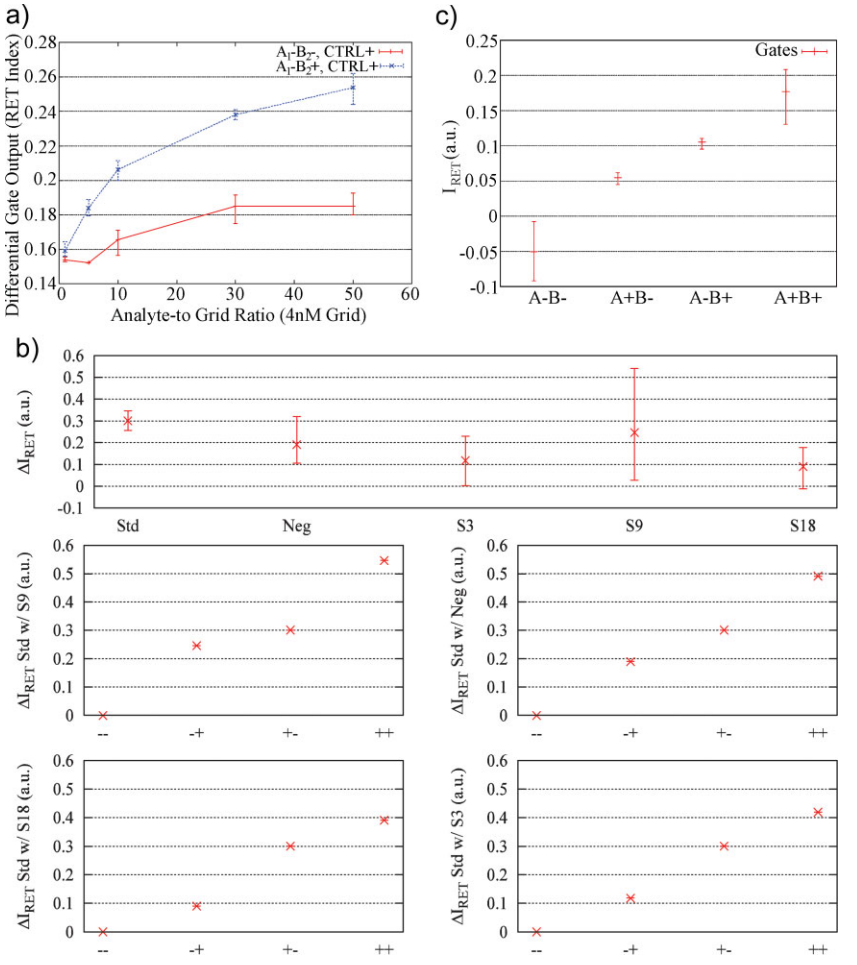

Figure 6. a) Sensitivity to various analyte concentrations. The observed change in I_{RET} for gate 1 and gate 2 is shown as a function of concentration for a DNA analyte (26-nt) that targets gate 2. The ratio of analyte to a fixed concentration of DNA grid (4 nM) is varied to achieve different analyte concentrations (4–200 nM). With an unsophisticated, portable, commercial CCD spectrometer and short exposures (≈2 min), the detection limit is approximately 4 nM at an analyte-to-grid ratio of 1:1. b) ΔI_{RET} response as a function of tether. The top panel shows the observed change in I_{RET} for five output tethers across three experiments. The lower panels show how each tether contributes a unique output signal when used with the standard (Std) tether by analytically combining the averages from the top panel. Each input condition (*x* axis) exercises a distinct combination of tethers. c) Dual gate output response. The two gates have identical input and output spectra with the exception that one uses the Std tether and the other uses the S18 tether. The data were collected from four experiments performed in triplicate.

input conditions over three identical tests. The gate type in this experiment permits the use of both donor emission bands for the I_{RET} calculation, unlike in the previous DNA/RNA/protein experiments, and the error bars are derived from the minimum and maximum samples. The response in Figure 5c clearly shows that the input conditions can be detected from an otherwise identical gate configuration by output tuning with a tether.

To understand more precisely how each gate output is disrupted by an analyte, nonlinear least-squares fitting of the observed change in I_{RET} is used to determine pre- and post-melt RET parameters such as κ^2 and r. To do this, we model our system as a population of gates and free chromophores. A yield factor, f_y, is the ratio of grid-bound to free chromophores and represents the extent to which we have ideally formed circuits. This leads to an observable fluorescence output rate (F_x') per gate of $F_x' = F_x \cdot f_y + E_x(1 - f_y)$. To account for analyte-independent disruption of gates during the melting process, we use a gate recovery factor, f_r, which quantifies the fraction of undamaged gates that bind analyte, in the fluorescence rate equation $F' = F_x \cdot f_y \cdot f_r + E_x(1 - f_y \cdot f_r)$.

Figure 7 shows the fit between the model and the data for pre- and post-melting of a sensor with two active gates targeting two DNA analytes (Supporting Information, Section 5). Since the functional yield must also be estimated in addition to the structural yield, we do not use the QSA or other AFM-derived yield metrics because we have found that commensurate binding between planar DNA nanostructures and flat surfaces artificially enhances the apparent yield. To obtain the best fit possible between the model and data, we first use data from two idle gates to characterize the fabrication yield of our system. The best fit for the idle-gate data estimates that approximately 35% of possible pairs of logic gates have formed correctly. This underscores the discrepancy induced by AFM and accepted methods to estimate yield,[35] which conclude that our gate yield, based on structural yield, should be closer to 47%.

To determine parameters such as the pre- and post-melt κ^2 and r for the active gate, we use the estimated circuit yield and solve for the best fit to F' allowing the gate recovery factor (f_r), separations ($r_{x,y}$), and orientations ($\kappa_{x,y}^2$) to vary between analyte types (e.g., DNA, RNA, or protein) but each to remain fixed across similar runs (e.g., $N>3$). The fitting results (see Figure 7) support the hypothesis that analyte binding disrupts gate outputs by modulating κ^2 rather than r, since separation plays such a limited role at short distances. Specific details for each fit can be found in the Supporting Information; Figure 7 presents the best fit when donor–acceptor pair distances and orientation can vary pre- and post-melt (the summed least-squares residual (LSR) is within 0.4% of the maximum data value). We note that to achieve the experimental ΔI_{RET} of ≈0.25, the inferred separations must be high (>5 nm) and the orientation factors similar to those for rigidly bound chromophores (<0.01). Since the chromophores we use are hydrophobic and susceptible to binding in the major groove of duplex DNA,[36–38] this suggests that a change in donor–acceptor orientation (or a combination of distance and orientation) is the most likely cause of output modulation because separation alone is unable to match the observed ΔI_{RET}.

NANO MICRO small

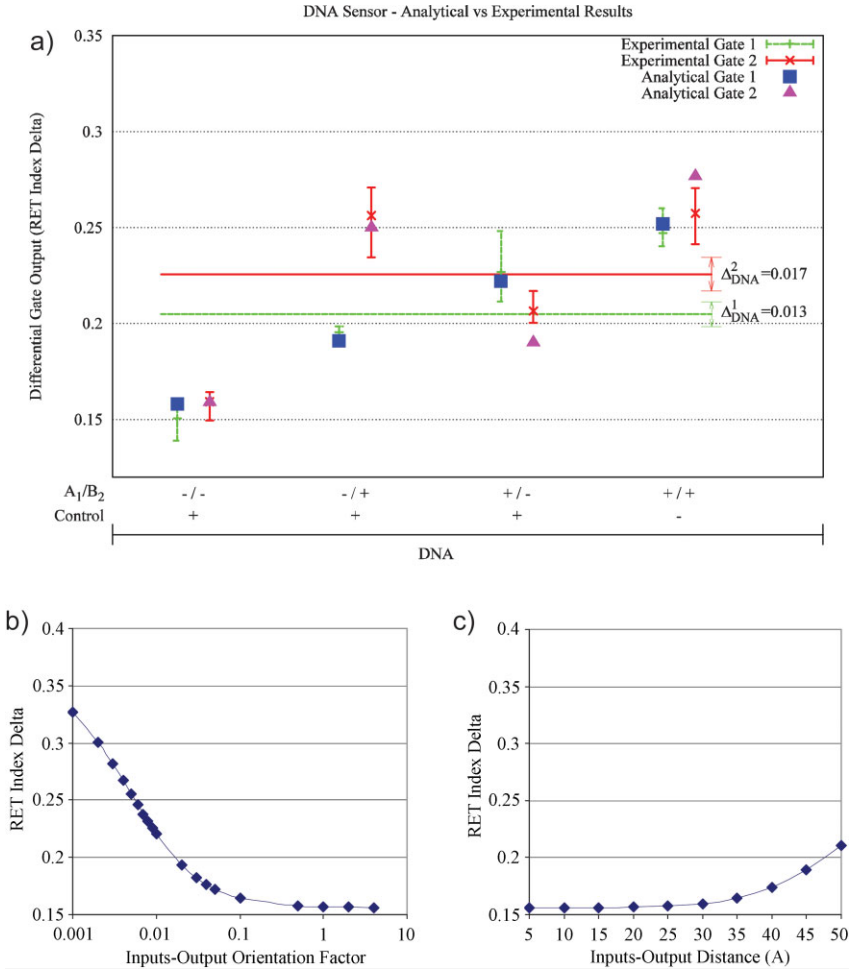

Figure 7. Fitting results. The best fit to F' is calculated by allowing the gate separations ($r_{x,y}$) and orientations ($\kappa_{x,y}^2$) to vary. a) The analytical result for DNA sensing is shown against the equivalent experimental results. b) The modulation is restricted to inputs-to-output orientations only and the $A_1^-B_2^+Ctrl^+$ configuration is calculated assuming varying orientation factors in the bound-analyte gate (*x* axis). c) The same scenario as in (b) but allowing only input–output separations to vary. Each *y* axis is the calculated ΔI_{RET}.

3. Conclusions

The methods described here demonstrate the feasibility of sensing biomolecules with RET logic. The method takes advantage of DNA self-assembly to build nanoscale grids with integrated RET circuits designed to operate as digital multiplexers. However, an important aspect of this work was to demonstrate viable pathways towards building larger RET circuits suitable for high-throughput sensing of many analytes, simultaneously. To do this, we used Boolean logic to create a multiplexer by designing logic terms that enable a distinct output for each unique sensor. Upon excitation, or addressing, we observed the output from one and only one kind of sensor. In this way, it is possible to combine many such sensors into a single monolith, smaller than the diffraction limit, as long as each address uniquely identifies a single kind of sensor.

The logprime-output-encoding technique described here trades signal-to-noise for address space by requiring a greater degree of significance in any measured response. Thus, single-photon-counting techniques, with an ability to detect attomoles of chromophores, dilute gates where the analyte is in excess, and a library of only six distinct chromophores (i.e., five inputs and one output) will enable sensing of over 24 analytes on a single 4×4 DNA grid. After accounting for yield (35%) and a diffraction-limited spot size of approximately 700 nm^2 (e.g., using 600-nm fluorescent output) the overall sensor density could be as high as 10^{13} m^{-2} unique analyte,s which currently exceeds the density of next-generation sensor arrays (e.g., gene chips with 500-nm-diameter probe spots) by an order of magnitude. More importantly, the approach we report here is a step towards integrating more complex RET logic onto nanoscale DNA grids that can be seamlessly integrated into biological assays.

Acknowledgements

We thank the National Science Foundation (CCF-07-02434, CCF-08-29911), AFRL (FA8750-05-1-0018-P000), DARPA (HR0011-09-1-0025), and ARO (W911NF-09-1-0478) for partial support of this work. We also thank Agilent Technologies for AFM equipment and fellowship support from Duke University.

[1] A. P. de Silva, S. Uchiyama, *Nat. Nanotechnol.* **2007**, *2*, 399–410.
[2] V. Balzani, A. Credi, M. Venturi, *ChemPhysChem* **2003**, *4*, 49–59.
[3] H. Tian, Q.-C. Wang, *Chem. Soc. Rev.* **2006**, *35*, 361–374.
[4] L. Gobbi, P. Seiler, F. O. Diederich, *Angew. Chem.* **1999**, *111*, 737–740; *Angew. Chem. Int. Ed.* **1999**, *38*, 674–678.
[5] R. Baron, O. Lioubashevski, E. Katz, T. Niazov, I. Willner, *Angew. Chem.* **2006**, *118*, 1602–1606; *Angew. Chem. Int. Ed.* **2006**, *45*, 1572–1576.
[6] D. Margulies, G. Melman, A. Shanzer, *J. Am. Chem. Soc.* **2006**, *128*, 4865–4871.
[7] D. Margulies, C. E. Felder, G. Melman, A. Shanzer, *J. Am. Chem. Soc.* **2007**, *129*, 347–354.
[8] M. N. Win, C. D. Smolke, *Science* **2008**, *322*, 456–460.
[9] G. Seelig, D. Soloveichik, D. Y. Zhang, E. Winfree, *Science* **2006**, *314*, 1585–1588.
[10] K. Rinaudo, L. Bleris, R. Maddamsetti, S. Subramanian, R. Weiss, Y. Benenson, *Nat. Biotechnol.* **2007**, *25*, 795–801.
[11] M. Heilemann, E. Margeat, R. Kasper, M. Sauer, P. Tinnefeld, *J. Am. Chem. Soc.* **2005**, *127*, 3801–3806.
[12] S. Habuchi, R. Ando, P. Dedecker, W. Verheijen, H. Mizuno, A. Miyawaki, J. Hofkens, *Proc. Natl. Acad. Sci. USA* **2005**, *102*, 9511–9516.

[13] D. S. Bradshaw, D. L. Andrews, *J. Chem. Phys.* **2008**, *128*, 144506.
[14] F. Remacle, R. Weinkauf, R. D. Levine, *J. Phys. Chem. A* **2006**, *110*, 177–184.
[15] J. Andreasson, S. D. Straight, T. A. Moore, A. L. Moore, D. Gust, *J. Am. Chem. Soc.* **2008**, *130*, 11122–11128.
[16] M. Heilemann, P. Tinnefeld, G. S. Mosteiro, M. G. Parajo, N. F. V. Hulst, M. Sauer, *J. Am. Chem. Soc.* **2004**, *126*, 6514–6515.
[17] Y. Ohya, K. Yabuki, M. Hashimoto, A. Nakajima, T. Ouchi, *Bioconjugate Chem.* **2003**, *14*, 1057–1066.
[18] Q.-H. Xu, S. Wang, D. Korystov, A. Mikhailovsky, G. C. Bazan, D. Moses, A. J. Heeger, *Proc. Natl. Acad. Sci. USA* **2005**, *102*, 530–535.
[19] C. Fan, K. W. Plaxco, A. J. Heeger, *Trends Biotechnol.* **2005**, *23*, 186–192.
[20] I. L. Medintz, A. R. Clapp, H. Mattoussi, E. R. Goldman, B. Fisher, J. M. Mauro, *Nat. Mater.* **2003**, *2*, 630–638.
[21] V. V. Didenko, *BioTechniques* **2001**, *31*, 1106–1121.
[22] Y. G. Ke, S. Lindsay, Y. Chang, Y. Liu, H. Yan, *Science* **2008**, *319*, 180–183.
[23] G. Zheng, F. Patolsky, Y. Cui, W. U. Wang, C. M. Lieber, *Nat. Biotechnol.* **2005**, *23*, 1294–1301.
[24] J. Hahm, C. M. Lieber, *Nano Lett.* **2004**, *4*, 51–54.
[25] F. Patolsky, G. Zheng, O. Hayden, M. Lakadamyali, X. Zhuang, C. M. Lieber, *Proc. Natl. Acad. Sci. USA* **2004**, *101*, 14017–14022.
[26] W. U. Wang, C. Chen, K.-H. Lin, Y. Fang, C. M. Lieber, *Proc. Natl. Acad. Sci. USA* **2005**, *102*, 3208–3212.
[27] E. Stern, J. F. Klemic, D. A. Routenberg, P. N. Wyrembak, D. B. Turner-Evans, A. D. Hamilton, D. A. LaVan, T. M. Fahmy, M. A. Reed, *Nature* **2007**, *445*, 519–552.
[28] C. Pistol, C. Dwyer, *Nanotechnology* **2007**, *18*, 125305–125309.
[29] J. SantaLucia, D. Hicks, *Annu. Rev. Biophys. Biomol. Struct.* **2004**, *33*, 415–440.
[30] R. S. Mathew-Fenn, R. Das, P. A. B. Harbury, *Science* **2008**, *322*, 446–449.
[31] A. Valoczi, C. Hornyik, N. Varga, J. Burgyan, S. Kauppinen, Z. Havelda, *Nucleic Acids Res.* **2004**, *32*, e175.
[32] R. Thomsen, P. S. Nielsen, T. H. Jensen, *RNA* **2005**, *11*, 1745–1748.
[33] P. C. Weber, D. H. Ohlendorf, J. J. Wendoloski, F. R. Salemme, *Science* **1989**, *243*, 85–88.
[34] L. Chaiet, F. J. Wolf, *Arch. Biochem. Biophys.* **1964**, *106*, 1–5.
[35] P. W. K. Rothemund, *Nature* **2006**, *440*, 297–302.
[36] K. A. Schallhorn, K. O. Freedman, J. M. Moore, J. Lin, P. C. Ke, *Appl. Phys. Lett.* **2005**, *87*, 033901.
[37] L. A. Fendt, I. Bouamaied, S. Thoni, N. Amiot, E. Stulz, *J. Am. Chem. Soc.* **2007**, *129*, 15319–15329.
[38] L. Strekowski, B. Wilson, *Mutat. Res.* **2007**, *623*, 3–13.

Received: October 22, 2009
Revised: January 26, 2010

